Optical measurement of biomechanical properties of individual erythrocytes from a sickle cell patient

Citation: Byun, HeeSu, Timothy R. Hillman, John M. Higgins, Monica Diez-Silva, Zhangli Peng, Ming Dao, Ramachandra R. Dasari, Subra Suresh, and YongKeun Park. "Optical Measurement of Biomechanical Properties of Individual Erythrocytes from a Sickle Cell Patient." Acta Biomaterialia 8, no. 11 (November 2012): 4130–4138.

As Published: http://dx.doi.org/10.1016/j.actbio.2012.07.011

Publisher: Elsevier

Persistent URL: http://hdl.handle.net/1721.1/101250

Version: Author's final manuscript: final author's manuscript post peer review, without publisher's formatting or copy editing

Published in final edited form as:
Acta Biomater. 2012 November ; 8(11): 4130–4138. doi:10.1016/j.actbio.2012.07.011.

Optical measurement of biomechanical properties of individual erythrocytes from a sickle cell patient

HeeSu Byun[a,1], **Timothy R. Hillman**[b,1], **John M. Higgins**[c,d], **Monica Diez-Silva**[e], **Zhangli Peng**[e], **Ming Dao**[e,*], **Ramachandra R. Dasari**[b], **Subra Suresh**[e], and **YongKeun Park**[a,*]

Ming Dao: mingdao@mit.edu; YongKeun Park: yk.park@kasit.ac.kr

[a]Department of Physics, Korea Advanced Institute of Science and Technology, Daejeon 305-701, Republic of Korea

[b]George R. Harrison Spectroscopy Laboratory, Massachusetts Institute of Technology, Cambridge, MA 02139, USA

[c]Center for Systems Biology and Department of Pathology, Massachusetts General Hospital, Boston, MA 02114, USA

[d]Department of Systems Biology, Harvard Medical School, Boston, MA 02114, USA

[e]Department of Materials Science and Engineering, Massachusetts Institute of Technology, Cambridge, MA 02139, USA

Abstract

Sickle cell disease (SCD) is characterized by the abnormal deformation of red blood cells (RBCs) in the deoxygenated condition, as their elongated shape leads to compromised circulation. The pathophysiology of SCD is influenced by both the biomechanical properties of RBCs and their hemodynamic properties in the microvasculature. A major challenge in the study of SCD involves accurate characterization of the biomechanical properties of individual RBCs with minimum sample perturbation. Here we report the biomechanical properties of individual RBCs from a SCD patient using a non-invasive laser interferometric technique. We optically measure the dynamic membrane fluctuations of RBCs. The measurements are analyzed with a previously validated membrane model to retrieve key mechanical properties of the cells: bending modulus; shear modulus; area expansion modulus; and cytoplasmic viscosity. We find that high cytoplasmic viscosity at ambient oxygen concentration is principally responsible for the significantly decreased dynamic membrane fluctuations in RBCs with SCD, and that the mechanical properties of the membrane cortex of irreversibly sickled cells (ISCs) are different from those of the other types of RBCs in SCD.

Keywords

Sickle cell disease; Red blood cell; Cell biomechanics; Cell membrane; Optical measurement

1. Introduction

Sickle cell disease (SCD) or sickle cell anemia is an inherited autosomal blood disorder characterized by abnormal mechanical and rheological behavior of red blood cells (RBCs).

*Corresponding authors. Tel.: +82 42 350 2514 (Y. Park).
[1]These authors contributed equally to this work.

SCD is caused by sickle hemoglobin (HbS), a variant hemoglobin (Hb) molecule resulting from a point mutation in the β-globin gene [1]. Upon deoxygenation, HbS polymerizes or self-assembles inside the RBC and significantly alters and damages the cytoskeleton and membrane cortex, resulting in a sickle-shaped RBC. This sickle RBC has decreased deformability, causing abnormal rheology in sickle blood and eventually various complications of SCD: ischemia and organ damage can result when microcirculation is impeded due to the poorly deformable RBCs. As a result of these complications and the limited choices for medical treatments, life expectancy for SCD patients is short; only 50% of patients with SCD survive beyond their fifth decade [2].

Characterization of the mechanical properties of RBCs is crucial to understanding the pathophysiology of many RBC-related diseases [3–5]. While the biochemistry of HbS is well understood, the mechanical properties of individual RBCs in SCD have not been fully assessed, largely due to the limitations of the measurement techniques [6]. Studies using filtration [7] or ektacytometry [8] have revealed that the sickle RBCs are stiffer than normal RBCs. However, these techniques cannot distinguish the mechanical properties of subpopulations of sickle RBCs or isolated RBCs, and they measure properties averaged over all RBCs in a blood sample. Micropipette aspiration [9], optical tweezers [10], the parallel-plate flow chamber method [11], and atomic force microscopy [12] have been employed to study the biomechanics of SCD at the cellular level. Although these methods have significantly enhanced our understanding of sickle cell biomechanics, none of them can probe all of the key mechanical parameters of individual RBCs simultaneously. Moreover, these previous methods rely on large, quasi-static external loads or perturbations to deform sickle RBCs through physical contact, and thus are not well suited to measure mechanical properties within linear deformation regimes.

Here we non-invasively investigate the biomechanical properties of individual RBCs in SCD by measuring the dynamics of membrane fluctuations in the sickle RBCs. Dynamic cell membrane fluctuations, consisting of nanometer-scale displacement of the cell membrane with millisecond temporal resolution, of the RBCs are strongly correlated with the structures of the cell membrane cortex and can be altered by biochemical changes [13–15]. To quantitatively measure the dynamics of membrane fluctuations for individual RBCs, we use an optical interferometric technique [13]. We analyzed the measured membrane fluctuations using a composite membrane model [13] in order to simultaneously retrieve four key mechanical properties of RBCs: bending modulus κ; shear modulus μ; area expansion modulus K_A; and cytoplasmic viscosity η.

2. Materials and methods

2.1. RBC sample preparation

Blood specimens were collected during the normal course of patient care at Brigham and Women's Hospital, Boston, MA, and used in experiments in accordance with a research protocol approved by the Partners Healthcare Institutional Review Board (IRB protocol number: 2006P000066). Samples were obtained from both a healthy individual and an SCD patient. The SCD patient was under treatment with hydroxyurea. The blood was collected in EDTA anticoagulant and stored at 4 °C. Clinical measurements of RBC volume and Hb concentration were made using an Advia 2120 automated hematology analyzer (Siemens Healthcare Diagnostics, Deerfield, IL).

Upon measurement, the blood samples, diluted with PBS (1:5 volume fraction), were sandwiched between two cover glasses. The RBCs were gently placed on glass plates and remained stationary during the measurements. The time period of examination for one group of samples was ~30 min. For each individual RBC, 256 frames of interferograms were

measured at 120 fps, which lasted ~2 s. All of the measurements were performed at room temperature.

2.2. Diffraction phase microscopy

The experimental setup for diffraction phase microscopy (DPM) is shown in Fig. 1. A diode-pumped solid-state laser (wavelength λ = 532 nm, 50mWoutput power, CrystaLaser, Reno, NV) was used as an illumination source for an inverted microscope (IX71, Olympus America Inc., Center Valley, PA). The microscope was equipped with a 60× objective lens (UIS2 PlanApo 60×, 1.42 NA, Olympus America Inc., Center Valley, PA), which facilitates a diffraction-limited transverse resolution of ~400 nm. A transmission grating (#46-072, Edmund Optics Inc. USA, 92 grooves mm^{-1}) was used to construct a common-path interferometry. With the additional optics used outside the microscope, the overall magnification of the DPM system was ~300×. A CMOS camera (FASTCAM 1024 PCI, Photron USA, Inc., San Diego, CA) was used to record interferograms.

2.3. Composite model of RBC

In order to retrieve key mechanical properties of RBCs from the measured membrane dynamic fluctuations, we used a continuum model of the composite spectrin-network/lipid membrane [16]. This model, incorporating the coupling between the bending and compression modes of the curved membrane, allows us to quantitatively determine the mechanical parameters of the cells. It has been experimentally validated with RBCs of different morphologies [13] and under different osmotic pressures [17]. The lipid bilayer, 4–5 nm thick, in the RBC membrane cortex can be mechanically characterized by a bending modulus κ and an area compression modulus K_A. On the cytoplasmic side of the membrane, the two-dimensional (2-D) triangular spectrin network is anchored to the bilayer via transmembrane proteins [18]. The mechanics of this spectrin network can be described as a 2-D elastic continuum having two equal Lamé constants, $\mu = \lambda$. The RBC cytosol primarily consists of Hb solution with viscosity η_C. Due to the high Hb concentration, η_C is significantly greater than the viscosity of the surrounding solvent, η_S. Thus, the mechanical description of the RBC model contains four important parameters, those identified in Section 1: κ, K_A, μ, η_C.

From an anatomical point of view, κ is thought to depend uniquely on the composition of the lipid bilayer, K_A on both surface tension in the bilayer and area modulus of the underlying spectrin network, and μ solely on the shear modulus of that network. The viscosity of the surrounding medium is fixed: η_S = 1.2 mPa s [19], and the viscosity of the highly concentrated cytosol solution η_C varies strongly with Hb concentration [20].

2.4. Analysis of spatial correlations of out-of-plane fluctuations

By analyzing the spatial correlations of the out-of-plane membrane fluctuations, the continuum model for RBCs facilitates the retrieval of key mechanical properties of RBCs from the membrane fluctuation data [13]. The spatial correlation function of the measured membrane fluctuations is calculated to be $C(d, t) = \langle \Delta h(d, t) \Delta h(0, 0) \rangle$, where the angular brackets denote averaging and d is a distance between two points on the RBC membrane. The temporal Fourier transformation of $C(d,t)$ is a power spectral density defined as $\bar{C}(d,\omega) = \infty\, C(d, t) e^{j\omega t} dt$, where ω is temporal angular frequency. According to the continuum model, it satisfies the equation:

$$\overline{C}(d,\omega) = 2k_B T/\omega \cdot (1 - d^2/4R^2) \sum_{l>0} \mathrm{Im}\,[\chi(l,\omega)] P_l\,(1 - d^2/4R^2) \quad (1)$$

where k_B is Boltzmann's constant, T the absolute temperature, $P_l(x)$ the Legendre polynomial of the lth order, R the effective radius of the RBC, $\chi(l, \omega)$ the out-of-plane response function, and d the distance between the two points. Full details of the model can be found elsewhere [13]. The response function χ relates the ambient thermal energy as a driving force to the RBC's response according to the fluctuation–dissipation theorem.

We adjust the four key parameters, κ, K_A, μ, and η_c, in order to obtain the best fit for $\bar{C}(d,\omega)$ between the measured data and the continuum model, through their influence on the response function χ. We constrain our fits by setting R to the average radius of curvature of the RBC obtained directly from the topographic image $\langle h(x, y)\rangle$ and fixing the viscosity of the extracellular medium to be η_s = 1.2 mPa s [19]. The elastic properties of the composite membrane are assumed to be dominated by reactive (i.e. non-dissipative) terms, so that we may treat the elastic constants as real and frequency-independent [13].

2.5. Comparison with other techniques

For the healthy RBCs, the optically measured mechanical properties are generally in good agreement with previous work [13]. The values for κ and μ for the healthy RBCs are consistent with the reports employing optical tweezers and micropipette aspiration techniques [9,21]. We note that our measured values for K_A for the healthy RBCs are in agreement with recent studies based on measuring the dynamic membrane fluctuation which reveal that K_A is in the range of 1–10 μNm^{-1} [22,23]. However, these values for K_A for the healthy RBCs are lower than the values reported from micropipette aspiration studies which find K_A to be in the range of 300–500 mN m^{-1} [21,24,25]. This large discrepancy between the micropipette-based technique and the measurement of dynamic membrane fluctuation can be rationalized by the fact that the former probes behavior dominated by the lipid bilayer and the latter deals with behavior dominated by the spectrin network. The RBC membrane consists of a fluid-like lipid bilayer and an underlying 2-D spectrin network. The K_A for an isolated lipid bilayer alone is in the range of 220–270 mN m^{-1} [26], with essentially zero shear resistance due to its fluid-like deformation. On the other hand, the direct measurement of K_A for the spectrin network was found to be 4.8 μNm^{-1}, roughly twice that of the shear modulus of the spectrin network (measured as 2.4 μNm^{-1}) [27]; this relationship of K_A/μ ~2 for a spectrin layer was also confirmed by theoretical predictions [28].

The micropipette-based techniques [29,30] essentially measure the whole cell's membrane K_A, where the entire RBC membrane, consisting of both the lipid bilayer and the spectrin network, is being stretched bi-axially. Since K_A of the spectrin network is several orders of magnitude lower than that of the lipid bilayer, under this loading condition, it is expected that K_A measured by the micropipette-based technique would be dominated by the K_A of the lipid bilayer. Therefore, the K_A for RBC measured by micropipette should be on par with the stand-alone lipid bilayer's K_A. We have verified this hypothesis using the established one-layer and two-layer RBC membrane model [31] and finite element method (FEM) simulations; see details in Appendix A.

The membrane fluctuation measurements probe local area compressibility, especially when extracted from a mapping of the membrane fluctuations with high spatial resolution, which is dominated by the properties of spectrin network. Since the anchoring points of the spectrin network to the lipid layer can move around within the lipid bilayer, the local area of the membrane is not strictly conserved; the lipid bilayer within a local area on the RBC membrane can be drawn from neighboring areas. The K_A of the RBC membrane measured by membrane fluctuations is thus expected to be dominated by the elasticity properties of the spectrin network, and consequently the ratio, K_A/μ ~2, should hold true theoretically for this type of measurement. Indeed, the area modulus of RBCs with normal discocyte shapes was found to be on the same order as that from the stand-alone spectrin network (obtained from

healthy RBCs); for all the different conditions measured in this study, we found that K_A/μ ~2 in each case. As an additional note, the micropipette experiment and theoretical model used for extracting RBC shear modulus [32] dominated by spectrin network elasticity are considerably different from the micropipette experiment and related mechanics model for extracting area expansion modulus [29,30]. A discussion of the details of these differences can be found in Ref. [32].

The measured RBC membrane properties would be determined by the combined effect of both lipid bilayer and the spectrin network. The lipid bilayer has negligible shear resistance, much lower than that of the spectrin network, while the spectrin network has a much weaker area expansion modulus than the lipid bilayer. Due to the fluid-like response of the lipid bilayer, it is well accepted that the shear resistance of the RBC membrane is provided solely by the spectrin network [33]. Note that when the two sub-layers of RBC membrane can slide relative to each other, then which sub-layer bears the majority of the load depends heavily on the loading conditions and stress states. For both micropipette measurements and membrane fluctuation measurements to extract the shear modulus, the dominant layer is the spectrin network. This results in comparable values for the shear modulus. The trend, however, is different for the area expansion modulus, where the dominant layer is the lipid bilayer for micropipette measurements and the spectrin network for the present membrane fluctuations measurements. For this reason, one would not expect the area modulus results measured from the present experiments to match those reported previously from techniques such as micropipette aspiration. In fact, these two techniques will be expected to provide vastly different values by virtue of the fact that they probe very different aspects of sub-cellular deformation, as indeed demonstrated in this work.

2.6. Relation between cytoplasmic viscosity and hemoglobin concentration

The cytoplasmic viscosity of RBCs depends on the Hb concentration in the RBC cytoplasm [20]. The translational diffusion coefficients for Hb and HbS monomer protein are described by an affine function of Hb concentration as follows; $D(c) = 7 - 0.128c$, where D is the translational diffusion coefficient in the unit of 10^7 cm^2 s^{-1} and c is the Hb concentration in units of g dl^{-1} [34]. When Hb remains as a monomer in viscous solution, $1/D$ can be linearly related to η/T (Stokes–Einstein equation) over a wide range of temperatures and solvent compositions, where T is the absolute temperature and η is the fluid viscosity [35]. Therefore, the relation between the cytoplasmic viscosity and the Hb concentration can be obtained as:

$$\eta = 0.0474T/(7-0.128c) \quad (2)$$

using known values of c (32 g dl^{-1}) and η (5.5 mPa s) measured for RBCs at physiological conditions.

2.7. Statistical analysis

A two-tailed, two-sample t-test between various test conditions was used to generate the p-values shown in the figures. The tolerances stated hereafter in the text represent one standard deviation over the ensemble of measured cells.

3. Results

3.1. Morphology of sickle RBCs

In order to measure quantitatively the morphology and dynamic membrane fluctuations of RBCs in SCD, we employ quantitative phase imaging (QPI) using DPM (see Section 2). DPM employs the principle of laser interferometry in a common-path geometry, and it

provides full-field QPI with high optical path-length stability [36,37]. The principle of QPI is shown in Fig. 2A. When a collimated beam passes through an RBC, the wavefront of the transmitted beam is changed due to the refractive index distribution in the RBC. The optical phase shift across the cell, $\Delta\varphi(x,y,t)$, can be quantitatively measured using laser interferometry. An interferogram of a sickle RBC measured by DPM is shown in Fig. 2B. From the measured interferogram, a quantitative phase image can be retrieved by using a phase extraction algorithm (Fig. 2C). The DPM optical path-length stability is 2.4 mrad, which corresponds to an RBC membrane displacement of 3.3 nm. Full details of the QPI of RBCs and the phase extraction algorithms can be found elsewhere [38,39].

Using DPM, we measured 50 RBCs from a healthy individual and 66 RBCs from an SCD patient ($n = 39$, 14, and 13 for types II, III, and IV, respectively, which are further described below) at ambient oxygen concentration (21%). From the measured quantitative phase image $\Delta\varphi(x,y,t)$, the cell height map can be retrieved; $h(x,y,t) = \lambda/(2\pi\cdot\Delta n)\cdot\Delta\varphi(x,y,t)$, where λ is the wavelength of the laser source and Δn the refractive index difference between RBC cytoplasm and the surrounding medium, $\Delta n = n_{Hb} - n_{medium}$. The main contribution to Δn is Hb, which is optically homogeneous in cytosol. It has been previously reported that the refractive index of HbS, n_{HbS}, is not significantly different from that of Hb, n_{Hb} [34]. This was confirmed by our flow cytometry measurement. We independently measured the mean cell volume (MCV) for the RBCs with SCD using an automated hematology analyzer (see Section 2). The hematology analyzer measures volume and Hb of individual RBCs based on elastic light scattering [40]. The mean cellular volume (MCV), mean cellular Hb concentration (MCHC), and mean cellular Hb content (MCH) for 66 sickle RBCs were measured as 96.8 fl, 34.7 g dl^{-1}, and 33.6 pg, respectively. Since the integration of optical phase delay over cell area can be related to MCV via the equation $MCV = \Delta n \iint \Delta\varphi dA$, we retrieve the value of the refractive index difference for HbS, $\Delta n = 0.06$ [41]. This value is consistent with previously reported values for Hb measured for healthy RBCs [15]. In addition, the MCV values for the sickle RBCs (96.8 fl) are higher than those for the healthy RBCs (80.1 fl) ($p < 10^{-3}$). The cell volume increase in sickle cell patients treated with hydroxyurea is consistent with previous reports [42]. There were no statistical differences in the MCV values between different morphological stages of the sickle disease ($p > 0.1$).

From the measurement of cell height as a function of time $h(x,y,t)$, we calculated time-averaged heights $\langle h(x,y)\rangle$ (Fig. 3A–D). Based on the morphological features, we classified the sickle RBCs into three groups: echinocytes (type II); discocyte (type III); and crescent-shaped irreversibly sickled cells (ISCs, type IV). These fractions of RBC cells in each of types II–IV into our classification are also consistent with those determined using an alternative classification system, separation by density [43].

3.2. Hb content of individual RBCs

The optical phase shift measured by QPI provides not only morphological information, but also information about the Hb content in individual sickle RBCs. Since the optical-path-length delay is determined by the dry mass of biological samples [41,44] and since the RBC consists mainly of Hb proteins (97% dry-mass fraction), the total optical path length delay in an RBC is linearly proportional to its total Hb content. To experimentally measure the constant of proportionality, we related the total optical phase path-length delay averaged from 66 sickle RBCs to the mean cellular hemoglobin (MCH) independently measured by the automated hematology analyzer.

The values of retrieved Hb content (mass) per cell are shown in Fig. 4. The mean value for healthy RBCs is 27.4 ± 2.7 pg, whereas the corresponding values for the types II, III and IV sickle RBCs are 36.0 ± 5.0, 28.5 ± 12.6, and 34.0 ± 6.3 pg, respectively. The values for the sickle RBCs are higher than that for the normal RBCs. Types II and IV sickle RBCs showed

a statistically significant difference when compared to the healthy RBCs ($p < 0.01$). The slight increase in the average Hb content (MCH) of sickle RBCs is consistent with prior studies showing that treatment with hydroxyurea results in the production of larger RBCs with the same Hb concentration and thus increases total MCH from 30.0 pg to 34.7 pg (by 16%) [45].

3.3. Dynamic membrane fluctuations in sickle RBCs

To probe the dynamic membrane fluctuations in the sickle RBCs, we calculated the membrane displacement map by subtracting the average height map from the instantaneous height map, $\Delta h(x,y,t) = h(x,y,t) - \langle h(x,y,t) \rangle$, (Fig. 3E–H, see SI movies S1–3). To quantitatively compare the membrane fluctuations, we calculated the standard deviation of the cell height fluctuations σ_h, that is, the root-mean-squared displacement. The values for σ_h were averaged over the cell area for 2 s at 120 frames s^{-1} (Fig. 5). Compared to the membrane fluctuation values of healthy RBCs (41.5 ± 5.7 nm), the membrane fluctuations of RBC in SCD are significantly less ($p < 10^{-3}$): 14.6 ± 9.1, 22.0 ± 8.4, and 18.6 ± 9.2 nm, for types II, III, and IV SCD, respectively. These reduced values for sickle RBCs also indicate decreased cell deformability.

3.4. Mechanical properties of RBCs in SCD

To investigate the biomechanical properties of sickle RBCs, we analyzed the membrane fluctuations with the previously developed viscoelastic continuum model [13,17] (see Section 2). By fitting the power spectral density function $\bar{C}(d,\omega)$ of the measured membrane fluctuation to the model, we quantitatively determined the mechanical parameters.

From these fits we determined the four biomechanical properties of RBCs in SCD (Fig. 5A–D). The mean value for κ for the healthy RBCs is 5.7 ± 1.6 k_BT, while the corresponding values for the types II, III and IV sickle RBCs are 7.4 ± 8.1, 10.4 ± 8.08, and 19.5 ± 7.4 k_BT, respectively (Fig. 5A). The RBCs in type-IV ISC show remarkably higher κ values when compared to the other three groups ($p < 0.01$). However, the mean values of κ for type II or III SCD RBCs are not statistically different from those of the healthy RBCs, despite their highly dispersed distributions. The absolute values of κ for sickle cells are different from those measured in a previous micropipette experiment [9] because of the differences in the loading conditions associated with the experimental methods, which will be discussed in detail below. However, the fact that κ for sickle-cell types II or III is not significantly different from that for normal RBCs is consistent with the previous report; the micropipette aspiration technique observed ~50% increases in the bending modulus for the most dehydrated sickle RBCs [9].

The shear modulus μ for the healthy RBCs is 7.1 ± 1.6 μNm^{-1}, and μ = 8.0 ± 4.3, 7.7 ± 4.9, and 20.0 ± 9.8 μNm^{-1} for types II, III, and IV SCD, respectively (Fig. 5B). Thus, similar to κ, the values of μ for type-IV ISCs are significantly higher than all other cell types ($p < 0.005$). However, also similar to the trend found for κ, the measured values of μ for type II or III SCD RBCs are not statistically different from those for the healthy RBCs. The present results for in-plane shear modulus values of healthy RBCs extracted from membrane fluctuation experiments are within the range of values obtained from other independent experimental techniques (e.g., Ref. [10]). These results are also consistent with previous reports where the values of μ for type II or III SCD RBCs were calculated as 6.7 ± 0.8 μNm^{-1} and the values for type IV SCD were 12.9 ± 2.5 μNm^{-1} [10].

The area expansion modulus K_A values are 15.4 ± 3.3 μNm^{-1} for healthy RBCs, with the corresponding values for types II, III and IV being 18.1 ± 11.9, 20.2 ± 14.8, 49.4 ± 29.7 μNm^{-1}, respectively (Fig. 5C). The measured K_A for healthy RBCs are in good agreement

with previous studies based on fluctuation-based measurements [22,23]. The values of K_A for ISCs are significantly different from those of other groups ($p < 0.005$). As is the case for κ and μ, despite the deviation in absolute values measured by a previous micropipette experiment, the observation that types II and III RBCs have similar values for K_A is consistent with a previous report [9]. In this previous study, the K_A values for the sickle RBCs were calculated to be ~2.5 times greater than the values for the healthy RBCs [9]. By comparison, our results show that the K_A values are 1.6 times (all II–IV type sickle RBCs) to 3.2 times (only type IV ISCs) greater than those of the healthy RBCs. As anticipated (and as discussed in Section 2.5), the absolute values of K_A obtained from the present membrane fluctuation experiment are markedly lower (by ~3–4 orders of magnitude) than those obtained from other techniques such as micropipette aspiration. This difference, as noted earlier, arises because these different techniques impose very different stress states and they sample different regions and sub-components of the cell. See Appendix A for further discussion on this point.

The values for η are 5.6 ± 1.6 mPa s for the healthy RBCs, with the values for types II, III, and IV SCD found to be 25.9 ± 9.8, 18.1 ± 8.5, 23.5 ± 5.4 mPa s, respectively (Fig. 5D). Thus, all types of SCD show significantly larger η (~fourfold) than healthy RBCs ($p < 10^{-3}$). However, the values for η are not statistically different among the three SCD RBC groups.

4. Discussion

This study presents the mechanical characterization of individual sickle RBCs under an oxygenated condition using a non-invasive optical measurement. In order to retrieve the mechanical properties, the dynamic membrane fluctuations of sickle RBCs measured by DPM were analyzed with a previously validated continuum model. With this approach, we have simultaneously and non-invasively estimated the four key mechanical properties of sickle RBCs with minimum perturbations. To confirm that this method can be used to extract the four mechanical properties, we also performed full three-dimensional (3-D) whole cell dissipative particle dynamics (DPD) simulations of RBC membrane fluctuations, using the same RBC membrane model as in Ref. [46]; the details of this exercise can be found in Appendix B.

For the healthy RBCs, the optically measured mechanical properties are generally in good agreement with previous reports. The values for κ and μ for the healthy RBCs are consistent with the previous reports employing optical tweezers and micropipette aspiration techniques [9,21].We note that our measured values for K_A for the healthy RBCs are in agreement with recent studies based on measuring the dynamic membrane fluctuation that find K_A to be in the range of 1–10 μNm^{-1} [22,23]. However, these values for K_A for the healthy RBCs are lower than the values reported from micropipette aspiration studies, i.e. in the range of 300–500 mN m^{-1} [21,24,25]. As discussed earlier in Section 2.5 in detail, this discrepancy between the micropipette-based method and the membrane fluctuation based technique can be attributed by the fact that the former tends to probe the lipid bilayer and the latter the spectrin network.

The present results also enable the identification of distinctive contributions of membrane rigidity and cytoplasmic viscosity with respect to different RBC types in SCD. Compared to healthy RBCs, the sickle RBCs in all morphological types (II–IV) showed significantly decreased cell deformability, which is also manifested in decreased dynamic membrane fluctuation. This decreased membrane fluctuation of RBCs in SCD is also consistent with a recent optical measurement where wide-field digital interferometry was used for QPI [47]. Such observations of the decreased deformability of sickle RBCs in oxygenated condition

agree with previous studies using filtration and ektacytometry [7,8] of cell populations. There were no significant differences in deformability among different groups in SCD, which is consistent with a previous report [48].

The results presented here indicate that the decreased deformability in non-ISC (types II and III) sickle RBCs, which is primarily a result of the abnormally high cytoplasmic viscosity in SCD, but not significantly of changes in membrane mechanical properties (κ, μ, and K_A). All types of sickle RBCs were found to exhibit nearly three to four times the cytoplasmic viscosity of normal RBCs (Fig. 6D). This high cytoplasmic viscosity in sickle RBCs may also explain the high bulk viscosity in sickle RBCs in the oxygenated condition [43].

For the case of ISCs, however, markedly higher membrane modulus values and high cytoplasmic viscosity contribute to decreased dynamic membrane fluctuation. Indeed, the values for κ, μ, and K_A of non-ISCs (type II and III) do not show appreciable differences from those of healthy RBCs; only the ISCs do. However, η values for all types of SCD RBCs are different from those of the healthy RBCs. Our results are consistent with a previous report that deformability is not different between SCD RBC cell types [48]. The present finding can also explain a previous experiment which indicated that deformability of sickle RBCs can be dramatically affected by cytoplasmic viscosity [49].

The increased cytoplasmic viscosity in SCD RBCs could be due to HbS polymer being present even at room oxygen concentration [48], or to the severe dehydration of dense sickle RBCs [50]. However, our independent measurement with a hematology analyzer showed that the value for MCHC for the SCDs in this study is 34.7 g dl^{-1}, which does not support the dehydration hypothesis, but instead, the possibility of the presence of HbS polymer.

Furthermore, the possible presence of HbS polymer is also consistent with our measured cytoplasmic viscosity. When Hb remains in viscous solution, the cytoplasmic Hb concentration can be obtained from the cytoplasmic viscosity using the Stokes–Einstein relation (see Section 2). Our measured values of the cytoplasmic viscosity for all types of SCD have average 23.8 ± 9.5 mPa s. These abnormally high values of viscosity correspond to Hb concentrations of 45.5 ± 4.5 g dl^{-1} using Eq. (2). This calculated Hb concentration is ~32% greater than that independently measured with the hematology analyzer (34.7 g dl^{-1}). The deviation between the measured and calculated values of viscosity (assuming purely viscous cytoplasm) suggests the possibility of the presence of HbS polymer in the SCD cytoplasm.

Higher cytoplasmic viscosity (higher Hb concentration) is not expected to affect the static mechanical properties of the healthy RBCs in which Hb remains in viscous solution. However, this is not true for sickle RBCs. A previous study has shown that the high cytoplasmic viscosity significantly decreases static deformability in sickle RBCs [9]. The decreased static and dynamic deformability of oxygenated sickle RBCs has been measured by using micropipette aspiration [10], ektacytometry [51], viscometry [7], and filtration techniques [52]. This decrease deformability is believed to have the following causes: (i) the membrane surface area to cell volume ratio is not a limiting factor for the dense sickle RBCs [10,51] and (ii) the deformability of the sickle RBCs can be dramatically improved when the cell hydration is normalized so that the sickle RBCs have normal cytoplasmic viscosity [49–51].

The increase of κ for ISCs indicates a less bendable lipid membrane, suggesting modifications in the structure or composition of the RBC membrane cortex (Fig. 6A). These structural interruptions of the sickle RBC membrane cortex could be caused by the formation of HbS polymer fibers under a deoxygenated condition, which results in exposure of trans-membrane protein epitopes and lipid exchange between the inside and the outside of

the sickle RBC [53]. It is also noteworthy that the values for κ, μ, and K_A of ISCs are significantly increased, unlike the non-ISCs. This can be rationalized on the basis of phospholipid destabilization [54] or membrane cytoskeletal dysfunction [55], which is limited to ISCs.

5. Conclusion

In this paper, we have reported the first complete characterization of all the relevant biomechanical properties of individual RBCs with SCD using a single, non-invasive optical measurement technique. The key mechanical properties of the sickle RBCs (bending modulus, shear modulus, area expansion modulus, and cytoplasmic viscosity) were measured simultaneously with minimum perturbation. The present method has the potential to provide further understanding of the pathogenesis and pathophysiology of SCD. For example, the study of the mechanism of sickle cell vaso-occlusion and rescue [56], adhesion of sickle RBCs to the endothelium [57], the role of ATP mediating and remodeling the RBC membrane structures [14,22,58], the effect of oxygenation and deoxygenation conditions on the biomechanical properties of the sickle RBCs [59], and the protective mechanism of SCD against malaria infection [60] could now be further accessible to direct, non-invasive, optical experimental study following the approach discussed here.

Supplementary Material

Refer to Web version on PubMed Central for supplementary material.

Acknowledgments

The authors wish to acknowledge Prof. Mahn Won Kim (KAIST), Prof. Philip A. Pincus (University of California, Santa Barbara), and Prof. George Karniadakis and Dr Xuejin Li (Brown University) for helpful discussions. This work was supported by National Institutes of Health (under grants 9P41-EB015871-26A1, R01HL094270 and DK083242) at MIT, and by KAIST, KAIST Institute for Optical Science and Technology, the Korean Ministry of Education, Science and Technology (MEST) grant No. 2009-0087691 (BRL), and National Research Foundation (NRF-2012R1A1A1009082). Partial support from the Infectious Diseases Interdisciplinary Research Group funded by the Singapore-MIT Alliance for Research and Technology (SMART) Center is also acknowledged. YKP acknowledges support from TJ ChungAm Foundation.

References

1. Stuart MJ, Nagel RL. Sickle-cell disease. The Lancet. 2004; 364(9442):1343–60.
2. Platt OS, Brambilla DJ, Rosse WF, Milner PF, Castro O, Steinberg MH, et al. Mortality in sickle cell disease – life expectancy and risk factors for early death. N Engl J Med. 1994; 330(23):1639–44. [PubMed: 7993409]
3. Diez-Silva M, Dao M, Han J, Lim C, Suresh S. Shape and biomechanical characteristics of human red blood cells in health and disease. MRS Bull: Mater Res Soc. 2010; 35(5):382.
4. Bao G, Suresh S. Cell and molecular mechanics of biological materials. Nat Mater. 2003; 2:715–25. [PubMed: 14593396]
5. Suresh S, Spatz J, Mills JP, Micoulet A, Dao M, Lim CT, et al. Connections between single-cell biomechanics and human disease states: gastrointestinal cancer and malaria. Acta Biomater. 2005; 1(1):15–30. [PubMed: 16701777]
6. Barabino G, Platt M, Kaul D. Sickle cell biomechanics. Annu Rev Biomed Eng. 2010; 12:345–67. [PubMed: 20455701]
7. Chien S, Usami S, Bertles JF. Abnormal rheology of oxygenated blood in sickle cell anemia. J Clin Invest. 1970; 49(4):623. [PubMed: 5443167]
8. Sorette MP, Lavenant MG, Clark MR. Ektacytometric measurement of sickle cell deformability as a continuous function of oxygen tension. Blood. 1987; 69(1):316. [published erratum appears in 1987;69(4):1272]. [PubMed: 3790727]

9. Evans E, Mohandas N, Leung A. Static and dynamic rigidities of normal and sickle erythrocytes. Major influence of cell hemoglobin concentration. J Clin Invest. 1984; 73(2):477. [PubMed: 6699172]
10. Nash GB, Johnson CS, Meiselman HJ. Mechanical properties of oxygenated red blood cells in sickle cell (HbSS) disease. Blood. 1984; 63(1):73–82. [PubMed: 6689955]
11. Barabino GA, McIntire L, Eskin SG, Sears DA, Udden M. Endothelial cell interactions with sickle cell, sickle trait, mechanically injured, and normal erythrocytes under controlled flow. Blood. 1987; 70(1):152. [PubMed: 3593962]
12. Maciaszek JL, Andemariam B, Lykotrafitis G. Microelasticity of red blood cells in sickle cell disease. J Strain Anal Eng Des. [accepted].
13. Park Y, Best C, Badizadegan K, Dasari R, Feld M, Kuriabova T, et al. Measurement of red blood cell mechanics during morphological changes. Proc Natl Acad Sci. 2010; 107(15):6731. [PubMed: 20351261]
14. Park YK, Best CA, Auth T, Gov N, Safran SA, Popescu G, et al. Metabolic remodeling of the human red blood cell membran. Proc Natl Acad Sci. 2010; 107:1289. [PubMed: 20080583]
15. Park YK, Diez-Silva M, Popescu G, Lykotrafitis G, Choi W, Feld MS, et al. Refractive index maps and membrane dynamics of human red blood cells parasitized by *Plasmodium falciparum*. Proc Natl Acad Sci. 2008; 105(37):13730. [PubMed: 18772382]
16. Kuriabova T, Levine AJ. Nanorheology of viscoelastic shells: applications to viral capsids. Phys Rev E. 2008; 77(3):031921.
17. Park YK, Best CA, Kuriabova T, Henle ML, Feld MS, Levine AJ, et al. Measurement of the nonlinear elasticity of red blood cell membranes. Phys Rev E. 2011; 83(5):051925.
18. Discher DE, Carl P. New insights into red cell network structure, elasticity, and spectrin unfolding – a current review. Cell Mol Biol Lett. 2001; 6(3):593–606. [PubMed: 11598637]
19. Hochmuth RM, Buxbaum KL, Evans EA. Temperature dependence of the viscoelastic recovery of red cell membrane. Biophys J. 1980; 29(1):177–82. [PubMed: 7260246]
20. Wells R, Schmid-Schonbein H. Red cell deformation and fluidity of concentrated cell suspensions. J Appl Physiol. 1969; 27(2):213–7. [PubMed: 5796309]
21. Evans E. New membrane concept applied to the analysis of fluid shear- and micropipette-deformed red blood cells. Biophys J. 1973; 13(9):941–54. [PubMed: 4733701]
22. Betz T, Lenz M, Joanny J, Sykes C. ATP-dependent mechanics of red blood cells. Proc Natl Acad Sci USA. 2009; 106(36):15312–7.
23. Gov N, Zilman AG, Safran S. Cytoskeleton confinement and tension of red blood cell membranes. Phys Rev Lett. 2003; 90(22):228101. [PubMed: 12857343]
24. Hochmuth RM, Waugh RE. Erythrocyte membrane elasticity and viscocity. Ann Rev Physiol. 1987; 49:209–19. [PubMed: 3551799]
25. Lelièvre J, Bucherer C, Geiger S, Lacombe C, Vereycken V. Blood cell biomechanics evaluated by the single-cell micromanipulation. J Phys III France. 1995; 5:1689–706.
26. Rawicz W, Olbrich K, McIntosh T, Needham D, Evans E. Effect of chain length and unsaturation on elasticity of lipid bilayers. Biophys J. 2000; 79(1):328–39. [PubMed: 10866959]
27. Lenormand G, Hénon S, Richert A, Siméon J, Gallet F. Direct measurement of the area expansion and shear moduli of the human red blood cell membrane skeleton. Biophys J. 2001; 81(1):43–56. [PubMed: 11423393]
28. Dao M, Li J, Suresh S. Molecularly based analysis of deformation of spectrin network and human erythrocyte. Mater Sci Eng C. 2006; 26(8):1232–44.
29. Evans EA, Waugh R. Osmotic correction to elastic area compressibility measurements on red-cell membrane. Biophys J. 1977; 20(3):307–13. [PubMed: 922122]
30. Evans EA, Waugh R, Melnik L. Elastic area compressibility modulus of red-cell membrane. Biophys J. 1976; 16(6):585–95. [PubMed: 1276386]
31. Peng ZL, Asaro RJ, Zhu Q. Multiscale simulation of erythrocyte membranes. Phys Rev E. 2010; 81(3):031904.

32. Chien S, Sung K, Skalak R, Usami S, Tözeren A. Theoretical and experimental studies on viscoelastic properties of erythrocyte membrane. Biophys J. 1978; 24(2):463–87. [PubMed: 728524]
33. Helfrich W. Elastic properties of lipid bilayers: theory and possible experiments. Z naturforsch C. 1973; 28(11–1):693–703. [PubMed: 4273690]
34. Jones C, Jhonson C Jr, Penniston J. Photon correlation spectroscopy of hemoglobin: diffusion of Oxy HbA and Oxy HbS. Biopolymers. 1978; 17(6):1581–93. [PubMed: 656555]
35. Phillies G. Translational diffusion coefficient of macroparticles in solvents of high viscosity. J Phys Chem. 1981; 85(19):2838–43.
36. Popescu G, Ikeda T, Dasari RR, Feld MS. Diffraction phase microscopy for quantifying cell structure and dynamics. Opt Lett. 2006; 31(6):775–7. [PubMed: 16544620]
37. Park YK, Popescu G, Badizadegan K, Dasari RR, Feld MS. Diffraction phase and fluorescence microscopy. Opt Exp. 2006; 14(18):8263–8.
38. Popescu G, Park Y, Choi W, Dasari R, Feld M, Badizadegan K. Imaging red blood cell dynamics by quantitative phase microscopy. Blood Cells, Molecules, and Diseases. 2008; 41(1):10–6.
39. Debnath SK, Park Y. Real-time quantitative phase imaging by spatial phase shifting algorithm. Opt Lett. 2011; 36(23):4677–9. [PubMed: 22139281]
40. Harris N, Kunicka J, Kratz A. The ADVIA 2120 hematology system: flow cytometry-based analysis of blood and body fluids in the routine hematology laboratory. Lab Hematol. 2005; 11(1): 47–61. [PubMed: 15790553]
41. Popescu G, Park Y, Lue N, Best-Popescu C, Deflores L, Dasari R, et al. Optical imaging of cell mass and growth dynamics. Am J Physiol: Cell Physiol. 2008; 295(2):C538. [PubMed: 18562484]
42. Ferster A, Vermylen C, Cornu G, Buyse M, Corazza F, Devalck C, et al. Hydroxyurea for treatment of severe sickle cell anemia: a pediatric clinical trial. Blood. 1996; 88(6):1960–4. [PubMed: 8822914]
43. Kaul D, Fabry M, Windisch P, Baez S, Nagel R. Erythrocytes in sickle cell anemia are heterogeneous in their rheological and hemodynamic characteristics. J Clin Invest. 1983; 72(1):22. [PubMed: 6874947]
44. Barer R. Determination of dry mass, thickness, solid and water concentration in living cells. Nature. 1953; 172(4389):1097–8. [PubMed: 13111263]
45. Rodgers GP, Dover GJ, Noguchi CT, Schechter AN, Nienhuis AW. Hematologic responses of patients with sickle cell disease to treatment with hydroxyurea. N Engl J Med. 1990; 322(15): 1037–45. [PubMed: 1690857]
46. Fedosov DA, Lei H, Caswell B, Suresh S, Karniadakis GE. Multiscale modeling of red blood cell mechanics and blood flow in malaria. PLoS Comput Biol. 2011; 7(12):e1002270. [PubMed: 22144878]
47. Shaked NT, Satterwhite LL, Telen MJ, Truskey GA, Wax A. Quantitative microscopy and nanoscopy of sickle red blood cells performed by wide field digital interferometry. J Biomed Opt. 2011; 16:030506. [PubMed: 21456860]
48. Hiruma H, Noguchi CT, Uyesaka N, Hasegawa S, Blanchette Mackie EJ, Schechter AN, Rodgers GP. Sickle cell rheology is determined by polymer fraction-not cell morphology. Am J Hematol. 1995; 48(1):19–28. [PubMed: 7832188]
49. Clark M, Mohandas N, Shohet S. Hydration of sickle cells using the sodium ionophore monensin. A model for therapy. J Clin Invest. 1982; 70(5):1074. [PubMed: 7130394]
50. Gulley ML, Ross DW, Feo C, Orringer EP. The effect of cell hydration on the deformability of normal and sickle erythrocytes. Am J Hematol. 1982; 13(4):283–91. [PubMed: 7158623]
51. Clark M, Mohandas N, Embury SH, Lubin BH. A simple laboratory alternative to irreversibly sickled cell (ISC) counts. Blood. 1982; 60:659. [PubMed: 7104492]
52. Messer M, Harris J. Filtration characteristics of sickle cells: rates of alteration of filterability after deoxygenation and reoxygenation, and correlations with sickling and unsickling. J Lab Clin Med. 1970; 76(4):537. [PubMed: 5458019]
53. Frenette PS, Atweh GF. Sickle cell disease: old discoveries, new concepts, and future promise. J Clin Invest. 2007; 117(4):850. [PubMed: 17404610]

54. Franck P, Bevers E, Lubin B, Comfurius P, Chiu D, den Kamp JAO, et al. Uncoupling of the membrane skeleton from the lipid bilayer. The cause of accelerated phospholipid flip-flop leading to an enhanced procoagulant activity of sickled cells. J Clin Invest. 1985; 75(1):183. [PubMed: 3965502]

55. Hebbel R. Beyond hemoglobin polymerization: the red blood cell membrane and sickle disease pathophysiology. Blood. 1991; 77(2):214–37. [PubMed: 1985689]

56. Higgins J, Eddington D, Bhatia S, Mahadevan L. Sickle cell vasoocclusion and rescue in a microfluidic device. Proc Natl Acad Sci. 2007; 104(51):20496. [PubMed: 18077341]

57. Hebbel RP. Perspectives series: cell adhesion in vascular biology. Adhesive interactions of sickle erythrocytes with endothelium. J Clin Invest. 1997; 99(11):2561. [PubMed: 9169483]

58. Ben-Isaac E, Park YK, Popescu G, Brown FLH, Gov NS, Shokef Y. Effective temperature of red-blood-cell membrane fluctuations. Phys Rev Lett. 2011; 106(23):238103. [PubMed: 21770546]

59. Nash GB, Johnson CS, Meiselman HJ. Rheologic impairment of sickle RBCs induced by repetitive cycles of deoxygenation–reoxygenation. Blood. 1988; 72(2):539. [PubMed: 3401593]

60. Cho S, Kim S, Kim Y, Park YK. Optical imaging techniques for the study of malaria. Trends Biotechnol. 2011; 30(2):71–9. [PubMed: 21930322]

Appendix A. Measurement of RBC area expansion modulus by the micropipette aspiration technique is dominated by lipid bilayer properties

We simulated the micropipette experiments for measuring area expansion modulus of RBCs [29,30], using the established one-layer and two-layer RBC membrane models [31] and the finite element method. The in silico micropipette experiments were numerically simulated using the following input parameters. For the two-layer model, the lipid layer had zero shear modulus, an area expansion modulus of $4.5\times10^5\ \mu Nm^{-1}$, and a bending modulus of 2×10^{-19} J, and the spectrin layer had a shear modulus of $10\ \mu Nm^{-1}$, an area expansion modulus of $20\ \mu Nm^{-1}$, and zero bending modulus. For the one-layer model, the effective RBC membrane had a shear modulus of $10\ \mu Nm^{-1}$, an area expansion modulus of $4.5\times10^5\ \mu Nm^{-1}$, and a bending modulus of 2×10^{-19} J. The initial RBC shape was modeled as a sphere due to osmotic swelling and its radius was given as 3.27 μm. The aspiration pressure ranged from 30 to 90 mmHg. The pipette radius was given as 0.668 μm. Once we numerically obtained the (large) deformation response of the RBC due to the (negative) applied micropipette pressure, the same procedure to extract area expansion modulus used in Refs. [29,30] was followed. The results from the one-layer model gave an effective area expansion modulus of $4.0\times10^5\ \mu Nm^{-1}$, and the two-layer model provided an effective area expansion modulus of $4.1\times10^5\ \mu Nm^{-1}$. Thus, the estimated moduli from both one-layer and two-layer models were comparable and they were reasonably close to the value assumed for the lipid bilayer, $4.5\times10^5\ \mu Nm^{-1}$. The result from the two-layer model also specifically showed that the micropipette aspiration method used in Refs. [29,30] mainly probes the lipid-layer area expansion modulus instead of the spectrin-layer value; we carefully considered these two sub-layers separately. For both the one-layer and two-layer model, varying the membrane or spectrin shear modulus from $10\ \mu Nm^{-1}$ to 5 or $20\ \mu Nm^{-1}$ resulted in less than ±5% changes in the extracted area expansion modulus, and all the results are within 13% of the lipid layer AEM as shown in Table A1.

Table A1

Micropipette measurement of area expansion modulus (AEM) studied using the one-layer and two-layer RBC membrane models.

Input shear modulus (μN m^{-1})	One-layer model		Two-layer model	
	Extracted AEM (μN m^{-1})	% Of lipid AEM	Extracted AEM (μN m^{-1})	% Of lipid AEM
5	3.9×10^5	87%	4.0×10^5	89%
10	4.0×10^5	89%	4.1×10^5	91%
20	4.1×10^5	91%	4.3×10^5	96%

The lipid bilayer AEM is given as 4.5×10^5 μNm^{-1} in the model.

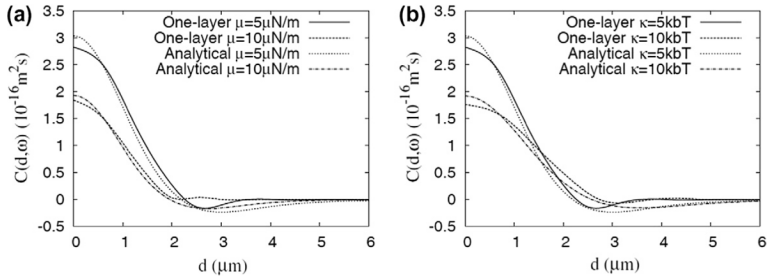

Fig. A1.

Height–height correlation as a function of projected distance predicted by the DPD model and the analytical model. (a) Effects of varying shear modulus μ (with K_a = 10 μNm^{-1}, κ = 5 k_bT, η = 0.008 Pa s), and (b) effects of varying bending modulus κ (with μ = 5 μNm^{-1}, K_a = 10 μNm^{-1}, η = 0.008 Pa s).

Appendix B. Membrane fluctuations measurement can be used to extract effective mechanical properties of the RBC membrane

To confirm that the analytical model and fitting algorithm used in the present study can be used to extract the four mechanical properties of the RBC membrane, we performed full 3-D whole cell dissipative particle dynamics (DPD) simulations of RBC membrane fluctuations, using the same RBC membrane model as in Ref. [46]. Fig. A1 shows the height–height correlation of dynamic RBC membrane fluctuations obtained using both the DPD model and the analytical model from the present study. The results obtained using the analytical model are very close to those obtained using the DPD model. This indicates that the “effective” mechanical properties of the RBC membrane (representing lipid bilayer and spectrin network as a single composite layer) are well captured by the analytical model. When we try to match the correlation function generated by the DPD model (solid line in Fig. A1a, computed with μ = 5 μNm^{-1}, K_a = 10 μNm^{-1}, κ = 5 k_bT, η = 0.008 Pa s) with our analytical model, the following set of values are found using the fitting algorithm used in the present study: μ = 4.4 μNm^{-1}, K_a = 8.2 μNm^{-1}, κ = 5.2 k_bT, η = 0.0087 Pa s, which agree well with the input properties of the effective membrane.

Appendix C. Figures with essential colour discrimination

Certain figures in this article, particularly Figs 1–6, are difficult to interpret in black and white. The full colour images can be found in the on-line version, at http://dx.doi.org/10.1016/j.actbio.2012.07.011.

Appendix D. Supplementary data

Supplementary data associated with this article can be found, in the online version, at http://dx.doi.org/10.1016/j.actbio.2012.07.011.

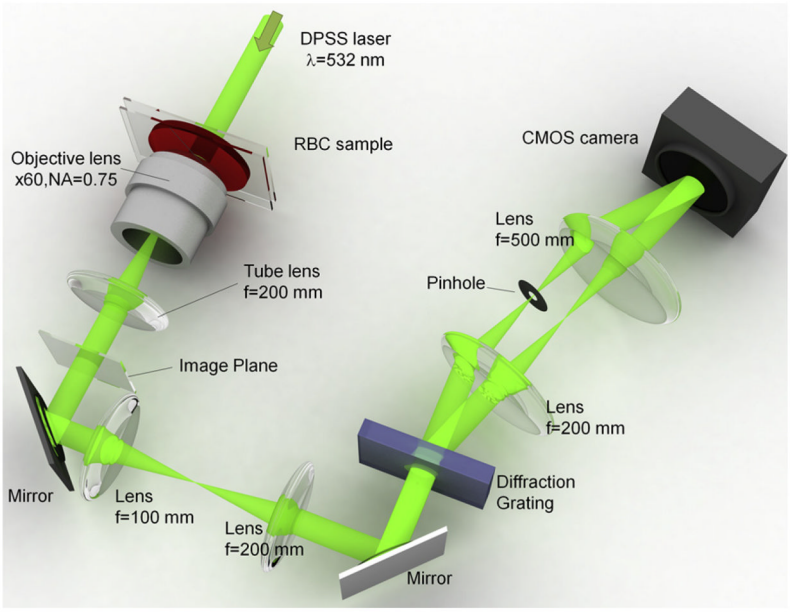

Fig. 1.
Experimental setup of DPM.

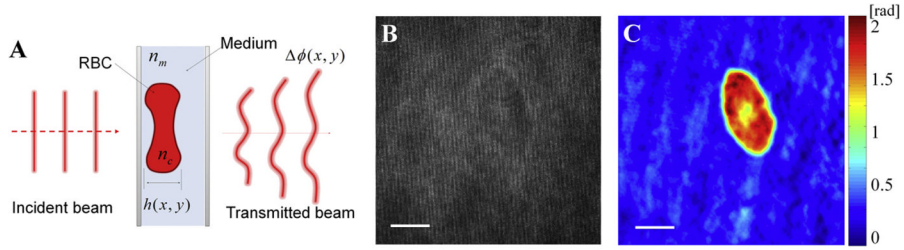

Fig. 2.

(A) Principle of QPI; $h(x,y)$ is the cell height map of an RBC; n_c and n_m are the refractive indexes of the RBC cytoplasm and the medium, respectively; $\Delta\varphi(x,y)$ is the phase delay map across the field of view. (B) Typical interferogram of a type IV sickle RBC (ISC) measured by DPM. (C) Retrieved phase image of (B). The scale bar is 5 μm.

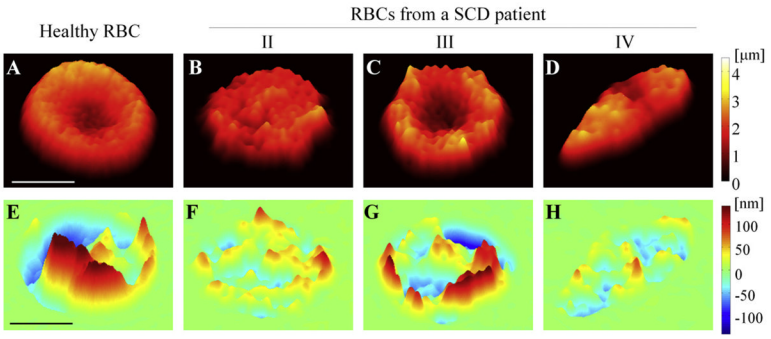

Fig. 3.

(A–D) Topographies of individual RBCs from healthy individuals (A), type II sickle cell (B), type III sickle cell (C), and type IV sickle cell (D). (E–H) Instantaneous membrane displacement maps of RBCs in (A–D). The scale bar is 5 μm.

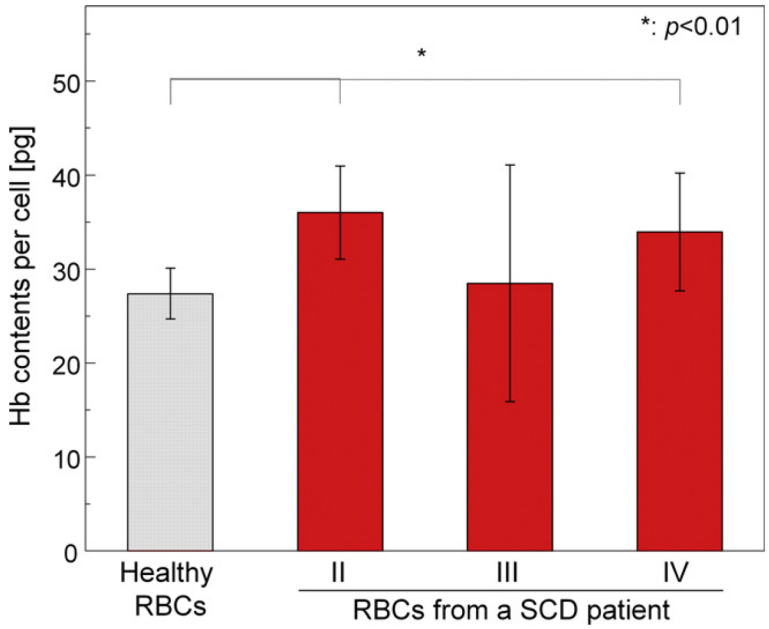

Fig. 4.
Hb content per cell measured by DPM.

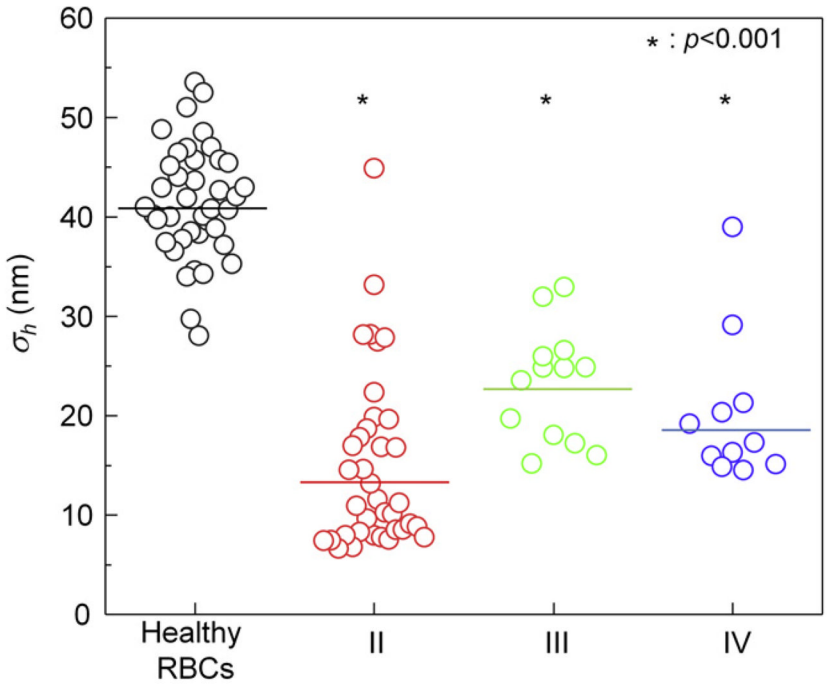

Fig. 5.

Membrane fluctuations for healthy, and types II, III and IV RBCs in SCD. Each data circle represents an individual RBC.

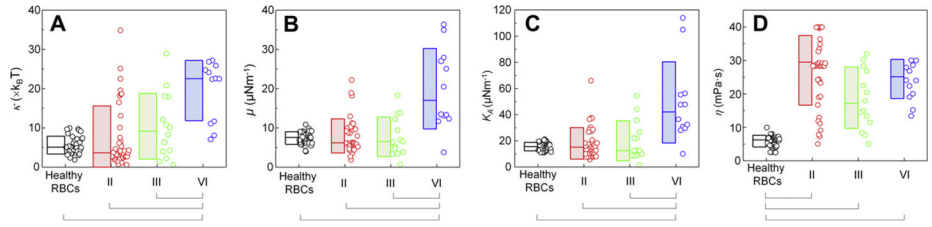

Fig. 6.

Measurements of (A) bending modulus κ, (B) Shear modulus μ, (C) area modulus K_A, and (D) viscosity η. The line between groups indicates significant difference ($p < 0.01$). The box represents the range within standard deviations and the solid line inside the box the average value.